International Journal of Greenhouse Gas Control 31 (2014) 138–152

Contents lists available at ScienceDirect

International Journal of Greenhouse Gas Control

journal homepage: www.elsevier.com/locate/ijggc

Optimizing heat integration in a flexible coal–natural gas power station with CO_2 capture

Charles A. Kang*, Adam R. Brandt, Louis J. Durlofsky

Department of Energy Resources Engineering, Stanford University, Green Earth Sciences Building, Stanford, CA, USA

ARTICLE INFO

Article history:
Received 28 January 2014
Received in revised form
17 September 2014
Accepted 22 September 2014
Available online 5 November 2014

Keywords:
MINLP
Bi-objective optimization
Price–duration curve
CO_2 capture retrofit
Heat recovery steam generator
Emission performance standard

ABSTRACT

Computational optimization is used to simultaneously determine the design and planned operating profile of a flexible coal–natural gas power station with CO_2 capture, under a CO_2 emission performance standard. The facility consists of a coal-fired power station undergoing retrofit with CO_2 capture. The CO_2 capture energy demand is provided by a specially designed combined cycle gas turbine (CCGT). The heat recovery steam generator (HRSG) component of the CCGT is modeled and optimized in detail, with explicit treatment of the discrete aspects of the HRSG configuration, including the number and sequential arrangement of HRSG internal components. Variable facility operations are represented by discrete operating modes selected based on the electricity price–duration curve. Two objectives, the minimization of capital requirement and the maximization of net present value, are considered in a bi-objective mixed-integer nonlinear programming formulation. Pareto frontiers, which define the optimal tradeoffs between these two objectives, are generated for six scenarios constructed from recent historical data from West Texas, the United Kingdom, and India.

For a 440 MW coal plant in a scenario based on 2011 West Texas data, the minimum effective net present cost required for the retrofit (which meets the CO_2 emission performance standard) varies from $278 to 383 million, and the minimum total capital investment requirement ranges from $346 to 517 million. The variations in these optimized values correspond to the range of the Pareto frontier within the bounds of the problem. The net present cost of the retrofit is less than the present value of the existing coal plant, $476 million, indicating that a retrofit is preferred over decommissioning. In the case of very low energy prices, however, decommissioning is shown to be the preferred option. The UK and India scenarios demonstrate that optimal designs can vary greatly depending upon location-specific economic conditions.

1. Introduction

In major economies around the world, a large number of coal-fired power plants exist with decades of life remaining. Furthermore, over 1400 GW of new coal-fired generation capacity was proposed to be added worldwide as of 2012 (Yang and Cui, 2012). Given the challenge of global climate change, reducing greenhouse gas emissions from these power plants is of great importance. Carbon dioxide capture and storage (CCS) can reduce CO_2 emissions from coal-fired power generation by up to 90% (Metz et al., 2005). Additionally, CCS could be applied to natural gas-fired electricity generation, which can effectively mitigate variability and intermittency associated with renewable power generation. Finally, CCS could also allow net capture of CO_2 from the atmosphere if combined with biofuels (Budzianowski, 2012). These facts suggest a possible long-term role for CCS in a low-carbon energy future.

Unfortunately, CCS has drawbacks. First, CCS has large capital costs. Second, CCS can reduce generation capacity for a plant by up to 30%, which may be problematic in regions with growing demand or with supply-constrained grids. Lastly, CCS does not generally improve generation flexibility, which is of concern because baseload operation likely will become less valuable, and generation responsiveness increasingly valuable, as renewable power generation increases.

In this paper we address these three challenges by optimizing the design and operation of an integrated coal-gas power station with CCS. This facility consists of an existing coal plant retrofitted with CO_2 capture. To overcome the supply reduction challenge, we model a CO_2 capture facility powered by an integrated combined cycle gas turbine (CCGT) system. In this 'auxiliary' concept, net electricity generation from the facility is increased instead of

* Corresponding author. Tel.: +1 650 479 6189.
E-mail addresses: cakcak@stanford.edu, charlesakang@gmail.com (C.A. Kang), abrandt@stanford.edu (A.R. Brandt), lou@stanford.edu (L.J. Durlofsky).

http://dx.doi.org/10.1016/j.ijggc.2014.09.019
1750-5836/

reduced as in 'parasitic' configurations. Our system uses a packaged heat- and power-integrated capture system based on mature CCGT technology, potentially reducing engineering costs compared to configurations that require site-specific retrofits. Finally, by using the CCGT to supply heat for the CO_2 capture process, we obtain operational flexibility that would not be achievable with many existing coal-fired power plants.

This paper focuses on heat integration optimization for coal-gas power stations with CCS. Thus, a key component of this work is the optimization of the design and operation of the heat recovery steam generator (HRSG). The HRSG, which is a major CCGT component, is a key driver of CO_2 capture economics because of the heat-driven nature of temperature-swing CO_2 capture technologies. In our formulation we model and optimize the HRSG configuration, including the number, size, and arrangement of HRSG elements. This results in a challenging mixed-integer nonlinear programming (MINLP) problem. We apply a bi-objective optimization framework to minimize the total capital requirement and maximize the net present value of the overall system. To our knowledge, within the context of CO_2 capture modeling, neither the detailed HRSG treatment applied here, nor the bi-objective optimization of the relevant MINLP problem, has been considered previously.

This paper proceeds as follows. We first outline previous work in this area along with our overall approach for modeling and optimization in Section 2. In Section 3, we describe our process and capital cost models, noting previous literature developments as appropriate. Verification of the process model and validation of the capital cost model are discussed in Section 4. We describe our representation of facility operations in Section 5, and present the optimization framework in Section 6. Results are discussed in Section 7, and we finish with concluding remarks in Section 8. We refer readers interested in further details on our modeling procedures to Kang et al. (2011) and to the online Supplementary Material (SM).

2. Overview of methods and approach

A number of investigators have previously applied computational optimization for the design and operation of power plants with CO_2 capture. Previous work includes studies addressing the design of CCGT facilities with CO_2 capture (Pelster, 1998; Pelster et al., 2001), the use of multi-objective optimization for power and cost in designing heat integration for a parasitic coal CCS retrofit (Harkin et al., 2012a,b), and the optimization of time-varying system operations (Cohen et al., 2012; Kang et al., 2011, 2012). Such studies have found value in CO_2 solvent storage (Versteeg et al., 2013; Kang et al., 2011), which can be used to time-shift the heat demands associated with solvent regeneration. Recent work has also applied computational optimization to coal plant parasitic CO_2 capture retrofit decisions, with coupled treatment of operations and design using a mixed integer linear optimization formulation (Khalilpour, 2014). Another group demonstrated a method to optimize design and operations of coal-fired power with parasitic CO_2 capture for minimum cost using dynamic process models (Mac Dowell and Shah, 2013). This work described the impact of CO_2 price on optimal designs, and found that the optimal CO_2 capture fraction was 95% for a 660 MW facility under certain economic conditions (Mac Dowell and Shah, 2013). In addition, optimization-based assessments have shown that the larger power system may benefit from flexible CO_2 capture because peak electricity demand could be met in part by temporarily shutting off CO_2 capture, thereby reducing capital outlay for new generation (Chen et al., 2010; Cohen et al., 2010).

In our previous work (Kang et al., 2011, 2012), we developed a modular representation of an integrated energy system consisting of several component models that interact by exchanging energy and mass flows. Those studies developed and applied procedures for the optimization of facility operation, but not for the optimization of facility design. Here, we optimize both the design and operations of similar types of integrated energy systems. Our facility burns coal and natural gas, and produces (among other outputs) electric power and CO_2, some of which is captured. For a given system, the costs include capital investment, fuel, operations and maintenance, and corporate income tax. The revenue from a planned operating profile is calculated by evaluating system power sales over time with a given time-varying electricity price profile. The optimization algorithm evaluates many ($\sim 10^6$) possible facility designs and operating profiles, systematically moving toward optimal solutions.

A major consideration in the design of such a facility is the interplay between capital cost and operating economics. Facility design and operations are inherently coupled: the valuation of a candidate facility design depends upon the way the facility is operated. Therefore, we solve for optimal facility design and operations jointly. The specific objectives considered are the minimization of total capital requirement (TCR) and the maximization of net present value (NPV). Other objectives could be specified, but these objectives allow us to quantify the tradeoffs between systems with low upfront investment (which are generally simple and inflexible) and systems with high NPV (generally more complex and flexible). Through use of a bi-objective optimization procedure we generate the Pareto frontier, which consists of system designs and operating profiles that are Pareto optimal. For Pareto-optimal solutions, improvement in one objective cannot be achieved without degradation in the other objective. Thus, our Pareto frontiers define the optimal tradeoffs between TCR and NPV.

The modular architecture of our model enables us to represent components with varying levels of complexity, and key components such as the HRSG are modeled in more detail than other components. We demonstrated earlier a preliminary form of this capability, in which continuous design parameters of the facility were determined algorithmically (using single-objective optimization) in coordination with operations (Kang et al., 2013). In this work, we improve the process models in several ways, and additionally optimize discrete design variables using a bi-objective MINLP procedure. The optimization applies a code recently developed within the context of oil field management, Particle Swarm Optimization–Mesh Adaptive Direct Search (PSO-MADS), that can handle unordered discrete optimization variables and bi-objective problems (Isebor, 2013; Isebor et al., 2013; Isebor and Durlofsky, 2014). Our method determines the optimal configuration (number and sequential arrangement) of HRSG internal components and the sizes of these components, while accounting for the effects of physical design specifications, such as tube diameters and fin heights, on efficiency and pressure drop.

3. Process model and system integration

The facility considered in this paper is shown in Fig. 1. A coal plant (CP, location 1 in Fig. 1) operates at baseload, producing constant power output. Coal plant flue gas, rich in CO_2, is scrubbed in the CO_2 capture unit (2). The CO_2 capture unit has a large demand for heat, which is supplied by steam drawn from the CCGT subsystem (3). We do not consider CO_2 transport and storage in this work, though cost estimates for these operations will be provided in Section 7.1.

The CCGT subsystem consists of three major units. A gas turbine (3a) burns natural gas, producing electric power and hot flue gas. The hot flue gas is used to generate steam in the HRSG (3b). Steam from the HRSG is expanded in steam turbines (3c), generating electricity. The condenser (3d) returns condensate to the HRSG. Steam

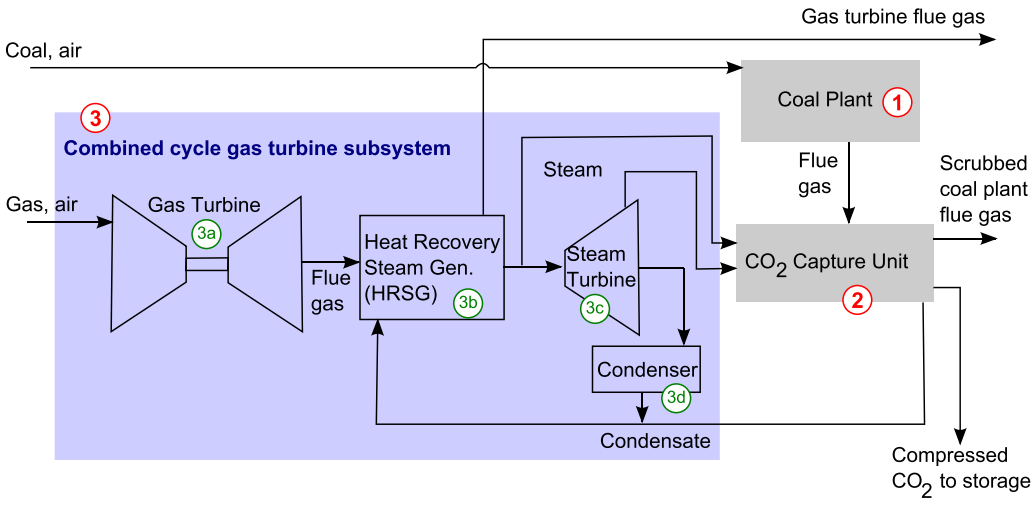

Fig. 1. Schematic of the overall facility.

can be drawn from the CCGT subsystem at several locations for use in the CO_2 capture unit.

Optimization decision variables include gas turbine capacity and number, CO_2 capture system capacity, and specification of the steam cycle including HRSG design. Because the focus of this work is in heat integration, we model and optimize the HRSG in substantial detail. Other system components are also optimized but are modeled at a higher level of abstraction. The process model is implemented in C++. We now describe the models of each of the major system components. Further details on the process models can be found in our earlier work (Kang et al., 2011) and in SM.

3.1. Coal plant (CP)

The model in Kang et al. (2011) of a pulverized coal power plant is used in this work. All environmental controls other than CO_2 mitigation are contained within the CP block. The CP has a capacity of 440 MW_e, and HHV efficiency of 36.3%. Coal properties differ across scenarios and are summarized in SM.

3.2. CO_2 capture system

An amine-solvent-based temperature-swing process is used for CO_2 capture. Our model includes heat and work requirements for solvent regeneration, compression, and pumping (pumps and blowers). We consider the default amine CO_2 capture design for a pulverized coal plant in IECM 8.0.2, and use data from IECM and other sources (Berkenpas et al., 2009; Rubin et al., 2007; Jassim and Rochelle, 2006). Regeneration heat duty is 3.68 MJ_{th}/kg CO_2. Compression work duty to pressurize the CO_2 to 13.8 MPa is 335 kJ_e/kg CO_2. Pump work duty for the solvent is 40 kJ_e/kg CO_2. We do not consider rich solvent storage in this work, although that can be used to time-shift the heat requirements for solvent regeneration.

We assume that the capture unit can be operated at partial load without a decrease in operational efficiency. Previously it has been shown that specific reboiler heat duty is not a strong function of operational partial loading (Ziaii et al., 2009a), and one study presented results indicating that reboiler heat duty may even improve somewhat under partial load (Arce et al., 2012). Furthermore, in our optimization results we found that Pareto-optimal designs did not exhibit strong use of partial load in the CO_2 capture system. Thus our model assumption of no efficiency loss with partial load in the CO_2 capture system has a minimal impact on our results. This is discussed further in Section 7.2.

3.3. Gas turbine

Our model includes a natural gas combustion turbine as described in Kang et al. (2011) and Kim (2004). The gas turbine (GT) has an HHV efficiency of 36.7%, specific power of 489 kJ/kg working fluid, and a flue gas outlet temperature at full load of 921 K, assuming an environment temperature of 298 K (Kang et al., 2011; Kim, 2004). In this work, the GT does not operate at partial load (i.e., it either operates at full capacity or it is shut off). In earlier work, which considered hour-to-hour operations and allowed for partial load GT operation, we found that this type of on-off behavior was often optimal (Kang et al., 2011).

3.4. Heat recovery steam generator (HRSG)

Because the CCGT subsystem requires a specialized HRSG design to provide the process heat demand for the CO_2 capture process, we employ modeling and optimization methods adapted from the literature on HRSGs. Classical optimization techniques (such as the Branch and Bound method for MINLP problems) have been applied to HRSG design previously (Manassaldi et al., 2011). Computational optimization has been applied to solve thermodynamic and thermoeconomic HRSG optimization problems (Casarosa et al., 2004). Two-step optimization has been used to optimize high-level design (i.e., HRSG pressures and temperatures) as well as detailed physical design (e.g., tube diameters) (Franco and Giannini, 2005, 2006). In addition, optimization has been used to identify functional relationships for optimal HRSG design under varying economic conditions (Godoy et al., 2011). In work that is methodologically similar to ours, a sophisticated two-stage approach for optimizing heat recovery steam cycles was applied to Shell's design for an integrated gasification combined cycle facility with CO_2 capture (Martelli et al., 2011), and to an integrated reforming combined cycle system (Martelli et al., 2012; Nord and Bolland, 2011). Net efficiency improvements of up to 0.5–0.9% out of 45.3% were attained (Martelli et al., 2012).

In previous HRSG optimization work, HRSG configuration—the number and ordering of HRSG components—generally is held fixed within an optimization run. Different configurations are typically considered through enumeration: several possible configurations are posited, and each is optimized separately. This is perhaps because it is difficult to manage the unordered discrete variables inherent to describing HRSG configurations. One group published a treatment of HRSG configuration optimization using a pruning process based on groups of related configurations called

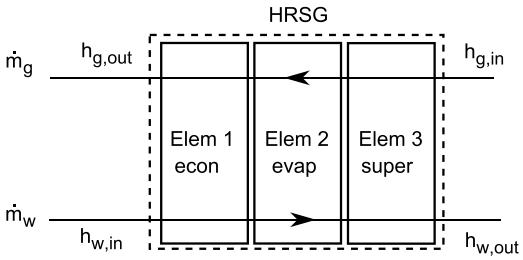

Fig. 2. Flows in a one-pressure HRSG.

'comprehensive layouts' (Mohagheghi and Shayegan, 2009), but this method is not fully general. Our method, in contrast to most previous approaches, optimizes HRSG configuration directly.

The HRSG is treated as a sequence of discrete heat exchangers ('elements'). We model the transfer of thermal energy from flue gas to water in a sequence of elements through which water and gas flow. This method of HRSG analysis and design has been used in thermodynamic and thermoeconomic studies on HRSGs and CCGTs (Mansouri et al., 2012; Woudstra et al., 2010), and in the optimization of these systems (Bassily, 2007; Franco and Russo, 2002; Kaviri et al., 2013; Norouzi et al., 2012).

HRSG elements are classified according to the state of the water stream, and are described by design water stream pressure p_{pl} [Pa] (pl denotes pressure level) and gas-side surface area A_g [m^2]. The four types of elements are economizers, evaporators, superheaters, and reheaters. In an economizer liquid water is heated, while in an evaporator water is boiled. In a superheater, steam is heated above the saturation temperature, and in a reheater, steam that has previously been expanded partially in a steam turbine is heated.

Fig. 2 shows a one-pressure HRSG consisting of one economizer, one evaporator, and one superheater. Flue gas enters from the right with high enthalpy and leaves with low enthalpy, transferring energy to the water stream. Water enters from the left as compressed liquid and exits as superheated steam on the right.

Substantial irreversibilities occur in one-pressure systems due to large temperature gradients between the gas and water streams. These occur in locations such as the gas inlet of the evaporator. Producing steam at two or more pressures can reduce the size of the temperature gradients and thereby reduce irreversibility and increase efficiency, at the cost of greater complexity and investment requirement. In HRSGs that generate steam at more than one pressure, multiple sets of economizers, evaporators, superheaters and/or reheaters are employed, with water streams of different pressures interleaved across elements.

Another consideration in HRSG design is the issue of gas-side pressure drop, Δp_{gas} [Pa]. This quantity is effectively a back pressure to the GT and can affect GT performance; with large Δp_{gas}, GT power output decreases (Zhao et al., 2003). Within the optimization, we apply a nonlinear constraint of $\Delta p_{gas} < 4.5$ kPa (cumulative over the entire HRSG) to ensure that HRSG back pressure does not negatively impact GT performance. We provide more details on our treatment of gas-side pressure drop in SM.

3.4.1. HRSG element

Each HRSG element is characterized by a 'heat transfer size' UA_g [W/K] and by the number of passes n_{pass}. The latter is a geometric property described in detail in SM. The quantity UA_g is the product of the overall heat transfer coefficient U [W/(m^2 K)] and the gas-side contact area of the HRSG element A_g. The coefficient U can be either a constant parameter or it can be calculated given the physical design specifications of the HRSG element. More details on U are provided in SM.

HRSG elements are modeled using algebraic relations. We use the effectiveness-number of transfer units method of heat exchanger analysis (Kays and London, 1984; Nellis and Klein, 2009; Shah and Sekulic, 2003) to determine the heat transfer within the element, $\dot{Q}_{actual}$ [W_{th}]. This necessitates the calculation of a nondimensional variable ε ($0 \le \varepsilon \le 1$), called effectiveness, that relates $\dot{Q}_{actual}$ to the theoretical maximum rate of heat transfer $\dot{Q}_{max}$ [W_{th}], where $\dot{Q}_{actual} = \varepsilon \dot{Q}_{max}$. The quantity ε is a function of HRSG element design and fluid states. Further information on HRSG element modeling is available in SM.

3.4.2. HRSG model

The states of all HRSG elements are coupled and must be determined simultaneously. Each element carries seven state variables, so a system with N_{elem} elements has $7N_{elem}$ state variables. The variables are the effectiveness ε, the mass flow rate of water $\dot{m}_w$ [kg/s], the enthalpies of the water at the inlet and outlet, $h_{w,in}$ and $h_{w,out}$ [J/kg], the temperatures of the gas at the inlet and outlet, $T_{g,in}$ and $T_{g,out}$ [K], and the overall heat transfer coefficient U. A typical three-pressure HRSG contains 10–14 elements.

Heat transfer and thermodynamic relationships within each of the HRSG elements provide four equations, giving a total of $4N_{elem}$ equations. The first such equation enforces energy conservation, while the second equation relates ε to the rate of energy transfer between the water and gas streams. The other two equations determine ε and U from the fluid states (alternatively, U can be specified as a constant).

Boundary conditions and links between elements provide $3N_{elem}$ equations. Boundary conditions include the water inlet temperature (from the condenser and/or CO_2 capture solvent regeneration reboiler), the flue gas inlet temperature (from the GT), and the evaporator water outlet enthalpy at each pressure level (given by the water saturation curve). The boundary conditions provide $(2 + N_{pl})$ equations, where N_{pl} is the number of HRSG pressure levels. Links between elements enforce conservation of mass, consistency in flue gas temperature between elements ($T_{g,in}$ of an element equals $T_{g,out}$ of the previous element), and consistency of water stream enthalpy between elements. The links between elements account for $(3N_{elem} - 2 - N_{pl})$ equations. Thus, we have a total of $4N_{elem} + (2 + N_{pl}) + (3N_{elem} - 2 - N_{pl}) = 7N_{elem}$ equations, so the system is well posed.

The nonlinear system of $7N_{elem}$ equations and $7N_{elem}$ unknowns is solved using a modified form of Newton's method. See SM for more details on the HRSG model.

3.5. Steam cycle

In a typical CCGT system, HRSG steam is fully expanded in steam turbines to a low condenser pressure to maximize electric power output. Typical condenser temperatures are approximately 300–350 K, depending on the availability of cooling. Expansions through multiple turbines are common, and are required for HRSGs that produce steam at more than one pressure.

Here, the steam exiting the HRSG can either be fully expanded, or it can be used to provide heat for CO_2 solvent regeneration. Steam can be extracted in a partially expanded state from the steam turbine chain, or diverted from the HRSG directly, bypassing the steam turbines. The facility uses water cooling, with the condenser modeled as a counterflow heat exchanger. We use a condenser temperature of 330 K. See SM for other details on the steam cycle.

3.6. Capital cost

Determining the optimal design of a facility requires accurate quantification of capital investment. We use the Guthrie method of capital cost estimation (Couper et al., 2008; Ulrich and Vasudevan, 2004, 2009). This cost estimate is prepared at the 'equipment-factored' level, corresponding to approximately

+30/−25% accuracy (Couper et al., 2008; Ulrich and Vasudevan, 2004).

In the Guthrie method, individual component 'purchased equipment costs' are estimated using an exponential scaling rule. All costs are adjusted for escalation using the Chemical Engineering Plant Cost Index (CEPCI) on a component-by-component basis. The purchased equipment costs are multiplied by 'module factors' to obtain 'bare module costs' of each component (Ulrich and Vasudevan, 2004). The component bare module costs are summed to give the facility bare module cost, which is then multiplied by a 1.18 contingency and fee factor to obtain the facility 'total module cost.' This is then multiplied by a 1.30 auxiliary facility factor to obtain the 'total capital cost' of the facility (Ulrich and Vasudevan, 2004). Interest during construction is calculated using uniform construction progress over three years, cost of capital equal to the discount rate, and backward escalation of project cost at the escalation rate, giving the total capital requirement (TCR). We use the same discount and escalation rates in the interest during construction calculation as in the NPV calculation described in Section 6.1, with numerical values provided in Section 7.1.

The exponential scaling rule used to estimate purchased equipment costs expresses the purchased equipment costs C [$] in terms of the size of the item S:

$$\frac{C}{C_{\text{ref}}} = \left(\frac{S}{S_{\text{ref}}}\right)^{\alpha}, \tag{1}$$

where C_{ref} [$] is the reference cost of the item, S_{ref} is the reference size of the item, and α is the scaling exponent. See SM for further details on the capital cost methodology.

4. Model verification and validation

We verified our HRSG and steam cycle models against several sets of results presented in the literature. Our model provides predictions of steam mass flow rate, steam temperature, and total heat transfer rate that match an existing reference solution to within 0.8% for a simple one-pressure system (Ganapathy, 1991). For a complex three-pressure system presented by Franco and Giannini (2006), our model (with calculated U values) produces predictions that deviate from the reference solution by 5.0% or less in all quantities. Detailed comparisons for these two systems are presented in SM.

To validate our capital cost model for the CCGT subsystem, optimization runs with maximization of NPV as the objective were performed for the CCGT. The components considered were the GT, HRSG, steam turbines, and condenser. In the range of 50–450 MW_e, the CCGT total capital cost determined by the model matched published values for actual constructed facilities (Gas Turbine World, 2010) to within 3.3% in all cases. Our model predictions for the cost proportions attributed to the different CCGT components are generally in accord with those given in publicly available sources (Kehlhofer et al., 1999; Ragland and Stenzel, 2000; Zhao et al., 2003), with our GT constituting a somewhat higher predicted proportion of cost than in the references. More detailed cost model validation is given in SM.

5. Operational model

The previous discussion concerned the system components and process models. We now consider the ways in which the facility can operate. Facility operations are represented by four mutually exclusive operating modes that are each allocated an operating duration in a year. Optimization is used to determine the duration in each of these modes. The modes (designated A–D) are as follows:

A. CCGT full power: In this mode, the GT(s) operate at full load. Steam is fully expanded to the condenser (p = 17.3 kPa, T_{sat} = 330 K), which maximizes steam cycle power output.
B. Steam extraction: The GT(s) operate at full load. Steam is partially expanded in the steam turbines and is then used for solvent regeneration in the CO_2 capture process (p = 300 kPa, T_{sat} = 407 K).
C. Steam diversion: The GT(s) operate at full load. Steam is used directly for solvent regeneration, bypassing the steam turbines.
D. Coal only: In this mode, the GT(s) do not operate and no steam is produced.

The four operating modes are well ordered in net electricity generation (sales), with mode A providing the most power and mode D providing the least. Modes A, B and C are well ordered in their CO_2 emission rates, with mode A having the greatest emissions rate and mode C having the least. The CO_2 emission rate [kg CO_2/s] in mode D is less than in mode A, but can be more or less than in modes B and C depending on the design of the overall system.

The solvent regeneration reboiler requires a heat source at $\gtrsim$400 K. For some designs, mode C involves the use of higher temperature steam for solvent regeneration in the CO_2 capture process; this may involve an additional heat exchanger in the CO_2 capture process. Because the cost of heat exchangers is only a small component of the cost of the CO_2 capture process, we do not include this cost in the model.

The treatment of modes B and C leads to a potential redundancy between these modes, and in fact a majority of optimized designs exhibited this redundancy. The potential redundancy occurs because mode C uses excess steam (steam beyond what the CO_2 capture unit can use) for power generation in the steam turbines. In systems in which mode B supplies enough steam to run the CO_2 capture unit at full capacity, this leads to redundancy between modes B and C: in such systems, both modes B and C operate the CO_2 capture unit at full capacity, so the two modes are equivalent. The systems that exhibit this redundancy thus do not have a mode that operates the CO_2 capture system at partial load. Therefore, it is possible for two systems that have different durations in modes B and C to exhibit identical performance metrics. This redundancy does not pose a problem for the optimizer.

The instantaneous optimal operating mode depends only on the operating profit associated with each mode. If the prices of fuel, operations and maintenance (O&M), electricity, and CO_2 emissions are known, then the optimal operating mode is the mode with the highest operating profit. Furthermore, for a given set of conditions, the first three modes are ordered optimally (A-B-C) in price of electricity, from high to low. Finally, under the conditions used in this study, the price of natural gas is low enough that mode D is preferred only at times with the lowest electricity prices. This ordering (A-B-C-D) holds for a CO_2 limit as well as for a CO_2 price because the constraint on CO_2 emissions induces an implicit shadow price for CO_2 emissions.

Fig. 3 shows a wholesale electricity price–duration curve, which consists of the hours of a year sorted by the wholesale market price of electricity. We use this curve to represent wholesale electricity market dynamics. The fact that the operating modes are well ordered in electricity price enables us to represent operations using threshold electricity prices, or 'strike prices,' which are the prices at which the operating mode switches. The strike prices shown in Fig. 3 are the operational decision variables and are determined algorithmically alongside the design variables.

Our use of the electricity price–duration curve in representing system operations prevents the model from including transient system behavior because the price–duration curve does not retain information about the sequential ordering of hours in time. Furthermore, in using hourly data in our operational model, we assume

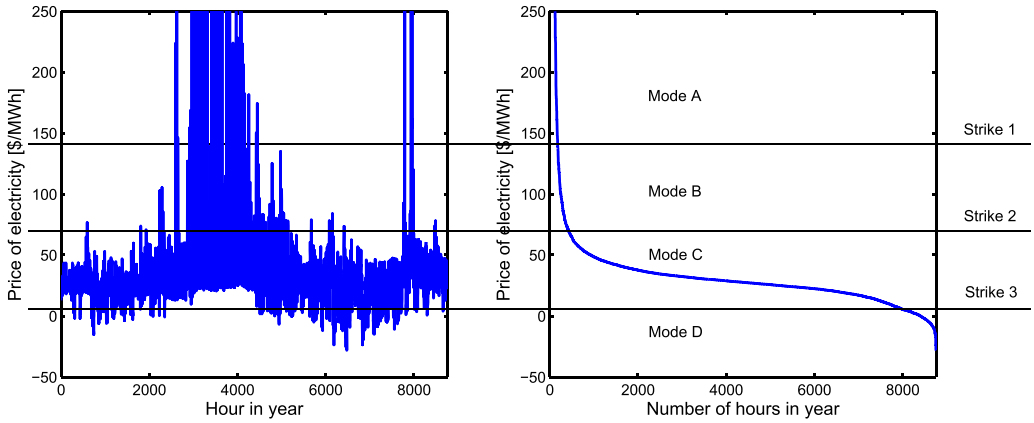

Fig. 3. Wholesale electricity hourly price (left) and price–duration curve (right), West Texas Hub Bus, 2011 (Electric Reliability Council of Texas, 2013).

that the auxiliary-powered CO_2 capture system can be controlled on an hourly time scale. We believe this assumption to be reasonable because it has previously been shown that CO_2 capture system transients typically dissipate on time scales of order one hour and that capture operations are not strongly affected by partial load plant operations (Chalmers and Gibbins, 2007; Chalmers et al., 2009; Brasington and Herzog, 2012; Ziaii et al., 2009b). We note that the downstream effects of flexible CO_2 capture can be managed in part by the use of CO_2 interim storage (Farhat and Benson, 2013).

6. Optimization formulation

As noted earlier, in this work operations and design are optimized simultaneously. This coupling is necessary because design affects the optimal planned operating profile, and the planned operating profile is necessary to evaluate the economics of a candidate design. We consider two objectives—maximization of net present value and minimization of total capital requirement—and pose the joint design and operation problem as a bi-objective MINLP problem of the following form:

$$\max_{\mathbf{u}_{\text{des}},\mathbf{u}_{\text{ops}}} \; [-C_{\text{TCR}}(\mathbf{x},\mathbf{u}_{\text{des}}),\, V_{\text{NP}}(\mathbf{x},\mathbf{u}_{\text{des}},\mathbf{u}_{\text{ops}})], \tag{2}$$

where

$$V_{\text{NP}}(\mathbf{x},\mathbf{u}_{\text{des}},\mathbf{u}_{\text{ops}}) = -C_{\text{TCR}}(\mathbf{x},\mathbf{u}_{\text{des}}) + P_{\text{op}}(\mathbf{x},\mathbf{u}_{\text{des}},\mathbf{u}_{\text{ops}})$$

subject to

$$\mathbf{u}_{\text{des}},\mathbf{u}_{\text{ops}} \in \Omega \tag{3}$$

$$\mathbf{h}(\mathbf{x},\mathbf{u}_{\text{des}},\mathbf{u}_{\text{ops}}) \le 0. \tag{4}$$

In this formulation, $\mathbf{x}$ indicates state variables, $\mathbf{u}_{\text{des}}$ indicates design decision variables, and $\mathbf{u}_{\text{ops}}$ represents operational decision variables (strike prices). The symbol C_{TCR} [$] designates total capital requirement, V_{NP} [$] is net present value, P_{op} [$] represents capitalized operating profits over the planned lifetime of the facility, Ω represents bound constraints on the decision variables, and $\mathbf{h}$ are general constraints, which can be nonlinear. These are discussed further in Sections 6.1 and 6.2.

Within the bi-objective optimization framework, we apply a PSO-MADS algorithm (Isebor, 2013; Isebor et al., 2013) to minimize a single objective derived from Eq. (2) (as explained below). The quantities C_{TCR}, V_{NP} and $\mathbf{h}$ are evaluated by repeated calls to the process model, which solves for the state variables $\mathbf{x}$. PSO-MADS is a derivative-free optimization algorithm built upon the open-source NOMAD project (Abramson et al., 2014; Audet et al., 2009; Le Digabel, 2011). It combines Particle Swarm Optimization (PSO, a stochastic global search method) with Mesh Adaptive Direct Search (MADS, a randomized direct search method). The algorithm proceeds by alternating between PSO iterations performed on a population of candidate solutions, and MADS iterations performed on the best PSO population member. By alternating between PSO and MADS in this way, the algorithm incorporates global exploration (through the PSO component) as well as convergence to a local optimum (provided by the MADS component). The procedure uses filter-based treatments to handle nonlinear constraints. With this approach, the aggregate constraint violation is minimized alongside the objective function (in a bi-objective fashion) to enforce constraint satisfaction.

Bi-objective optimization is accomplished here by performing a sequence of single-objective optimizations. The goal is to trace the Pareto frontier, which defines the set of Pareto-optimal solutions (as defined previously). The 'single-objective product formulation' (SOPF) (Audet et al., 2008) is applied for this purpose. PSO-MADS is used as the underlying optimization algorithm, and the overall framework, explained in detail in Isebor (2013) and Isebor and Durlofsky (2014), is referred to as BiPSOMADS.

The procedure entails first optimizing the two individual objectives, denoted f_1 and f_2, separately. In the following illustration, the goal is to maximize each of these objectives. The solutions computed during these optimizations provide a very coarse approximation to the Pareto frontier. Fig. 4(a) illustrates the result after the maximization of f_1, and Fig. 4(b) shows the result after the subsequent maximization of f_2. The region in which the Pareto frontier is the least resolved is then identified, and this enables the determination of the so-called reference point $\mathbf{r}$, which lies below the current estimate of the Pareto frontier in objective function space.

In the next step of BiPSOMADS, we search for solutions that maximize the 'distance' from the reference point. Fig. 4(c) illustrates the procedure after the first SOPF maximization. Here distance is defined as the product of the squared differences between the objective functions and the corresponding components of $\mathbf{r}$. Specifically, the single objective D we seek to maximize is given by:

$$D(\mathbf{x}) = (\max[0, f_1(\mathbf{x}) - r_1])^2 (\max[0, f_2(\mathbf{x}) - r_2])^2, \tag{5}$$

where f_1 and f_2 are the values of the two objective functions and r_1 and r_2 are the coordinates of the reference point in objective function space. The results of this optimization provide improved resolution of the Pareto frontier. The region in which the Pareto frontier is the least resolved is then identified, and this provides the next value of $\mathbf{r}$. This process (determine $\mathbf{r}$, perform a PSO-MADS run to maximize D in Eq. (5), update the estimate of the Pareto frontier) is continued until a stopping criterion is reached, which could be a specified number of PSO-MADS runs or a particular level of resolution in the Pareto frontier.

Our bi-objective optimizations are accomplished in two stages. We first run BiPSOMADS, as described above, to provide an estimate

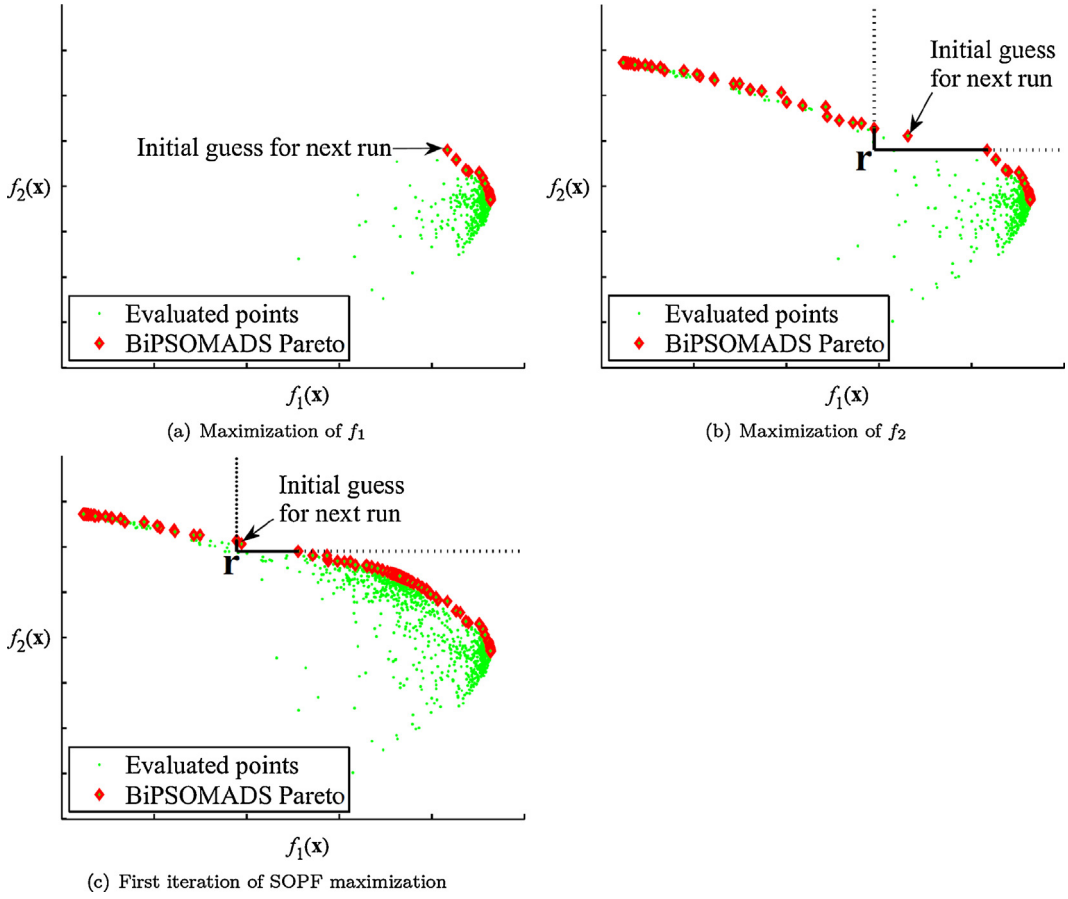

Fig. 4. Pareto frontier approximations after three BiPSOMADS steps. Adapted from Isebor and Durlofsky (2014).

of the Pareto frontier, using several initial guesses. In each BiPSOMADS run, ten PSO-MADS runs are performed. Because the frontiers associated with our problems can be complex and 'patchy,' and because regions of particular interest are not always sufficiently resolved by the initial ten PSO-MADS runs, we then identify a number of additional points to be used as initial guesses for second-stage BiPSOMADS runs. Following these runs, the final Pareto frontier is constructed from the combined results of all BiPSOMADS optimizations. The total number of BiPSOMADS optimization runs performed to obtain each Pareto frontier was in the range of 12–16.

In this work, all optimizations were run using parallel computation. In each BiPSOMADS run we typically accessed 20–50 computational cores.

6.1. Objective functions and decision variables.

We use two objective functions: TCR, which is minimized, and NPV, which is maximized. The latter is calculated based upon cash flows received at midyear over 30 years:

$$V_{\mathrm{NP}} = -C_{\mathrm{TCR}} + \sum_{y=0}^{29} \frac{0.85(R_{\mathrm{elec}} - C_{\mathrm{fuel}} - C_{\mathrm{O\&M}})(1+r_{\mathrm{esc}})^{y+0.5} - C_{\mathrm{tax},y}}{(1+r_{\mathrm{disc}})^{y+0.5}}, \tag{6}$$

where R_{elec} [$] is revenue from electricity sales in one year, C_{fuel} [$] is the total cost of fuel in one year, $C_{\mathrm{O\&M}}$ [$] is the total cost of operations and maintenance in one year, r_{esc} is the escalation rate, $C_{\mathrm{tax},y}$ [$] is the corporate income tax paid in each year, and r_{disc} is the nominal discount rate. Data for the calculation of $C_{\mathrm{O\&M}}$, which includes both fixed and variable O&M, are provided in SM. The coefficient of 0.85 to the pre-tax operating profit ($R_{\mathrm{elec}} - C_{\mathrm{fuel}} - C_{\mathrm{O\&M}}$) accounts for the capacity factor of the CP (the CCGT and CO_2 capture system only operate when the CP is operating). The quantity $C_{\mathrm{tax},y}$ varies yearly and is calculated from the pre-tax operating profit, with depreciation allowance, using a combined federal and state corporate income tax rate of 40%. Depreciation is evaluated using the 20-year 150% declining balance method, mid-quarter convention (Internal Revenue Service, 2013; Islegen and Reichelstein, 2011).

The optimization problem contains discrete (integer and categorical) and continuous decision variables. All decision variables are collected in a single vector and treated using BiPSOMADS. Table 1 provides a list of the optimization variables along with bound constraints. For a system with up to three HRSG pressure levels and 14 elements, we have a total of 42 decision variables (26 continuous variables and 16 discrete variables).

The integer variables are the number of gas turbines n_{GT} (this is also the number of HRSGs because we have one HRSG for each gas turbine) and the number of pressure levels n_{pl}. The categorical variables are the specification of type and pressure level of each element in the HRSG, $\mathbf{e}_{\mathrm{pl,type}}$. The domain of $\mathbf{e}_{\mathrm{pl,type}}$ is the Cartesian product of the possible types of HRSG elements (economizer, evaporator, superheater, reheater) and the possible pressure levels of the elements (1, 2, 3), with an additional setting to indicate deactivation of the element.

The continuous variables are total gas turbine capacity $n_{\mathrm{GT}} s_{\mathrm{GT}}$ [MW_e], CO_2 capture facility capacity C_{cap} [kg CO_2/s], water pressure at each HRSG pressure level p_{pl} [Pa], high pressure reheat steam pressure $p_{\mathrm{HP,rh}}$ [Pa], pressure of steam extraction p_{ext} [Pa],

Table 1
Optimization decision variables

Variable	Type	Symbol	# Vars	Units	Lower bound	Upper bound
Number of GTs	Integer	n_{GT}	1	–	1	3
Total GT capacity	Real	$n_{GT}s_{GT}$	1	MW	1	400
HRSG # press. levels	Integer	N_{pl}	1	–	1	3
HRSG steam pressures	Real	p_{pl}	3	Pa	1×10^5	19×10^6
HRSG extract press.	Real	p_{ext}	1	Pa	3×10^5	5×10^6
HRSG HP reheat press.	Real	$p_{HP,rh}$	1	Pa	1×10^5	20×10^6
HRSG element type &pl	Categ.	$\mathbf{e}_{pl,type}$	14	–	−1	11
HRSG nondim. elem. size	Real	$a_{g,0}$	1	–	0.1	3
HRSG rel. elem. sizes	Real	$\mathbf{a}_{g,rel}$	14	–	0.1	3
CCS relative capacity	Real	c_{cap}	2*	Fraction	0.0	0.9
Strike prices	Real	$\mathbf{d}_{sp}$	3	$/MWh	(0, −20, −30)	(200, 150, 100)

* One variable for absorption and one variable for regeneration and compression. These two variables converge to the same value during optimization.

variables controlling the HRSG element gas-side surface areas $\mathbf{A}_g$ [m^2], and strike prices $\mathbf{d}_{sp}$ [$/MWh]. Reheat is only allowed in three-pressure systems, for the highest pressure level. Note that the total GT capacity is a decision variable, and that the capacity of each individual GT is calculated with all GTs being identical.

We found that a better search was obtained by decomposing the HSRG element surface areas into $\mathbf{A}_g = A_{g,0}\mathbf{a}_{g,rel}$ where $A_{g,0}$ [m^2] is the HRSG element characteristic gas-side surface area and $\mathbf{a}_{g,rel}$ are relative HRSG element surface areas for each element. Furthermore, it is convenient to express $A_{g,0}$ as related proportionally to the gas turbine size; i.e., $A_{g,0} = a_{g,0}s_{GT}/\kappa$, where $a_{g,0}$ is the nondimensional HRSG element size and $\kappa = 9162\ W_e/m^2$ is a constant chosen such that $a_{g,0}$ takes on values of order one. The decision variables for the HRSG element surface areas are then $a_{g,0}$, which controls the overall size of the HRSG, and $\mathbf{a}_{g,rel}$, which controls the size of each element.

The HRSG has a predefined set of slots for HRSG elements. Associated with each slot i are one categorical variable ($e^i_{pl,type}$) and one continuous variable ($a^i_{g,rel}$). If the categorical variable of a slot indicates that it is deactivated, the continuous variable has no effect on the HRSG design.

The CO_2 capture capacity is expressed in nondimensional terms as $c_{cap} = C_{cap}/\dot{m}_{CP,fgCO_2}$, where $\dot{m}_{CP,fgCO_2}$ [kg CO_2/s] is the CP flue gas CO_2 emission rate. We implemented c_{cap} as two variables, one representing absorption capacity and the other representing regeneration and compression capacity. Over the course of an optimization run these two variables converge to the same value.

6.2. Optimization constraints

Three kinds of constraints apply to the facility. The first class of constraints ensure that the HRSG design is physically valid; candidate designs that violate these constraints are discarded. The second class of constraints are bound and linear constraints on the decision variables that limit the search space. The third class of constraints are general constraints applied to model-calculated quantities. These constraints enforce physical design standards and CO_2 policy requirements, and many of them are related to HRSG states. Below we describe the CO_2 policy constraints. See SM for a full listing of the other constraints.

We use an emission performance standard of 499 kg CO_2/MWh (1100 lb/MWh). This is the level that the US Environmental Protection Agency has proposed for new coal power plants (Environmental Protection Agency, 2013). In this study, we investigate the impact of the application of this standard to an existing CP, so the CP would need a CCS retrofit to continue operating. The emission performance standard applies to CO_2 emission intensity, which is calculated as E/G [kg CO_2/MWh] where E [kg CO_2] is the amount of CO_2 emitted and G [MWh] is the amount of electricity exported to the power grid. We can also treat other CO_2 regulations such as a carbon price without difficulty.

The emission performance standard acts as a constraint applied to each of the following system emission intensities:

Entire facility: Emission intensity of the entire facility including CP, CCGT, and CO_2 capture
Scrubbed CP: Emission intensity calculated from coal plant net power output (440 MW_e) and scrubbed CO_2 emissions
CCGT: Emission intensity calculated from the power output of GT(s) and CCGT steam turbines, and CO_2 emissions from the GT(s).

All of these emission intensities must be below 499 kg CO_2/MWh. The constraint is applied in this way to prevent 'diluting' CP emissions with the inherently less CO_2-intensive CCGT system. The CO_2 capture electricity demands are attributed to the facility as a whole, not to either of the major subsystems.

7. Results and discussion

7.1. Scenario construction

We constructed six scenarios (one base scenario and five sensitivity scenarios) from historical data. The four US scenarios are based around West Texas, which we selected in part because this region has a large amount of grid-connected wind power, and so may be representative of future power systems. Our other two scenarios are based on the United Kingdom and India. We used a nominal discount rate of $r_{disc} = 11.0\,\%/y$, and an escalation rate of $r_{esc} = 3.3\,\%/y$. We assume that the coal plant already exists and thus constitutes a sunk cost that does not affect the retrofit decision, so we do not include the CP capital cost in the objective functions. Therefore, the coal plant NPV involves only revenue, operating expenses, and corporate income tax.

The economic scenario has a substantial impact on the optimal decisions, with the economic parameters in different scenarios leading to substantially different designs and objective function values. The sensitivity of the results to economic assumptions suggests that it will be important to use a robust approach for economic forecasting. Despite the wide range of designs and objective function values, our procedure performs well for all scenarios considered.

The scenario data are shown in Table 2. We constructed the base scenario (WTX-Base) electricity price–duration curve, displayed in Fig. 3, using hourly day-ahead electricity market prices for the West Texas Hub Bus in 2011 (Electric Reliability Council of Texas, 2013). We used a natural gas price equal to the average price of gas delivered to U.S. electric power generators in 2011 (Energy Information

Table 2
Scenario parameters.

Scenario name	P_{elec} mean [$/MWh]	P_{elec} std. dev. [$/MWh]	$P_{nat.\ gas}$ [$/GJ] ([$/MMBtu])	P_{coal} [$/GJ] ([$/MMBtu])	CCS capital cost multiplier
WTX-Base	40.73	126.74	4.48 (4.73)	1.34 (1.41)	1.00
WTX-HighCapCost	40.73	126.74	4.48 (4.73)	1.34 (1.41)	1.25
WTX-HighEnergyCost	55.62	126.74	6.12 (6.46)	1.34 (1.41)	1.00
WTX-LowEnergyCost	24.27	40.65	3.21 (3.39)	1.34 (1.41)	1.00
UK	74.83	13.53	8.60 (9.08)	5.20 (5.49)	1.00
India	72.29	24.42	11.56 (12.20)	1.10 (1.16)	1.00

Administration, 2013). The coal price was $1.34/GJ ($1.41/MMBtu), which is approximately the long-run average price of Wyoming Powder River Basin coal delivered to Texas (Energy Information Administration, 2012, 2014).

The three West Texas sensitivity scenarios are high CCS capital cost (WTX-HighCapCost), high energy prices (WTX-HighEnergyCost), and low energy prices (WTX-LowEnergyCost). In constructing the scenario WTX-HighCapCost, we applied a constant multiplier of 1.25 to the capital cost of the CO_2 capture facility, while holding all other prices the same as in WTX-Base. The scenario WTX-LowEnergyCost was constructed using electricity prices for the West Texas Hub Bus in 2012 (Electric Reliability Council of Texas, 2013) and the corresponding 2012 average natural gas price for electricity (Energy Information Administration, 2013). To construct the scenario WTX-HighEnergyCost, we added $1.64/GJ ($1.73/MMBtu, corresponding to an increase of 36.5%) to the WTX-Base natural gas price, and $14.89/MWh (a 36.5% increase in terms of average price) to the WTX-Base electricity prices. Coal prices were not modified in this scenario. We constructed WTX-HighEnergyCost in this way to account for correlation between electricity and natural gas prices.

We developed two international scenarios using data for the United Kingdom and India in the year 2011. The UK scenario used half hour (averaged to hourly) electricity reference price data in 2011 given by the UK power market (APX Group, 2014). The India scenario used hourly average day-ahead market wholesale electricity prices from an Indian power market for the Gujarat-Maharashtra pricing area in 2011 (Indian Energy Exchange Ltd, 2014). Natural gas prices for the year 2011 were drawn from the FERC LNG Market Archives (Federal Energy Regulatory Commission, 2013), which includes data on landed gas prices in the United Kingdom and India. The price for UK natural gas from this source is essentially the same as for the UK National Balancing Point trading hub. Coal prices for the year 2011 were taken from the IEA Medium-Term Coal Market Report 2012 (International Energy Agency, 2012), which includes data for average coal price delivered to power plants in Northwest Europe and India.

As mentioned in Section 3, our model does not include costs associated with CO_2 transport or storage. If the captured CO_2 were to be transported by pipeline and stored in an onshore saline aquifer, the cost would be approximately $4–21 million/y using a combined transport and storage cost of $3–15/tonne CO_2 (Metz et al., 2005; Grant et al., 2013). This amounts to a net present cost of transport and storage of $47–249 million (excluding tax implications, which would tend to decrease this net present cost). This cost is not included in the results presented in this section. If the captured CO_2 were used for enhanced oil recovery, the cost for transport and storage could be much lower or even negative.

Further details on scenario construction, including currency conversions and fuel properties, are provided in SM.

7.2. West Texas

The existing coal plant without CCS has a NPV of $476 million in WTX-Base. As we will see, this is greater than the NPV of any system with CCS. Performing CO_2 capture thus represents an overall cost to the owner: the difference between the NPVs of the retrofitted systems and the NPV of the coal plant alone can be interpreted as the net present cost associated with meeting the emission performance standard by performing an auxiliary CCS retrofit. Importantly, however, the NPVs for optimal systems in the base scenario are still positive, indicating that the CO_2 capture retrofit is preferred to simply decommissioning the coal plant in response to the CO_2 regulation.

During the course of the optimization, 4.66×10^6 candidate designs were evaluated, of which 1.52×10^5 were unique and feasible. From these we construct a Pareto frontier for minimum TCR and maximum NPV, shown in Fig. 5. The Pareto frontier defines the optimal tradeoff between NPV and TCR, with each point on the frontier representing a different system (design and operational settings). From any point on the Pareto frontier (Pareto-optimal points), no improvement in one objective can be obtained without a degradation in the other objective. Non-Pareto-optimal points in Fig. 5 are shown only as gray '×'s, while Pareto-optimal points are marked with colored symbols, with symbol and color indicating the number of HRSG pressure levels. Note that the frontier is smooth in some regions, but discontinuous and 'patchy' in other regions. Some discontinuities in the frontier in Fig. 5, such as that between the one-pressure (blue open circles) and two-pressure systems (red open squares), are due to the discrete nature of the design space. Other discontinuities may result from the fact that our search is not exhaustive. More resolution in the frontier could be achieved by performing additional PSO-MADS runs, but because the general features of the solution are clearly evident in Fig. 5, this was not attempted here.

Given a plot such as that in Fig. 5, the decision maker would choose which Pareto-optimal point to implement based on his or

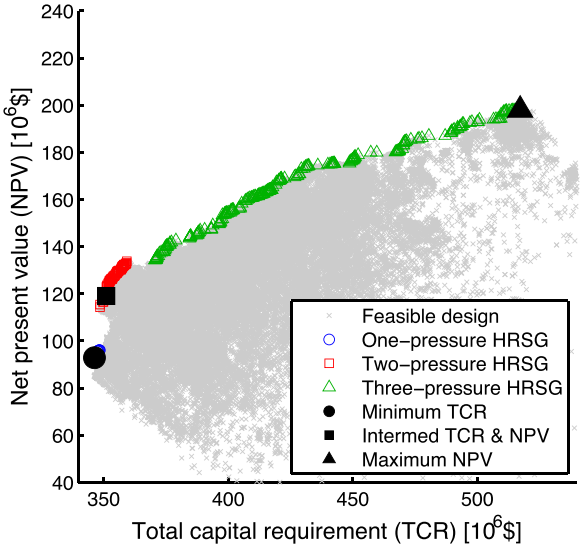

Fig. 5. Pareto frontier for base scenario (WTX-Base). (For interpretation of the references to color in text, the reader is referred to the web version of the article.)

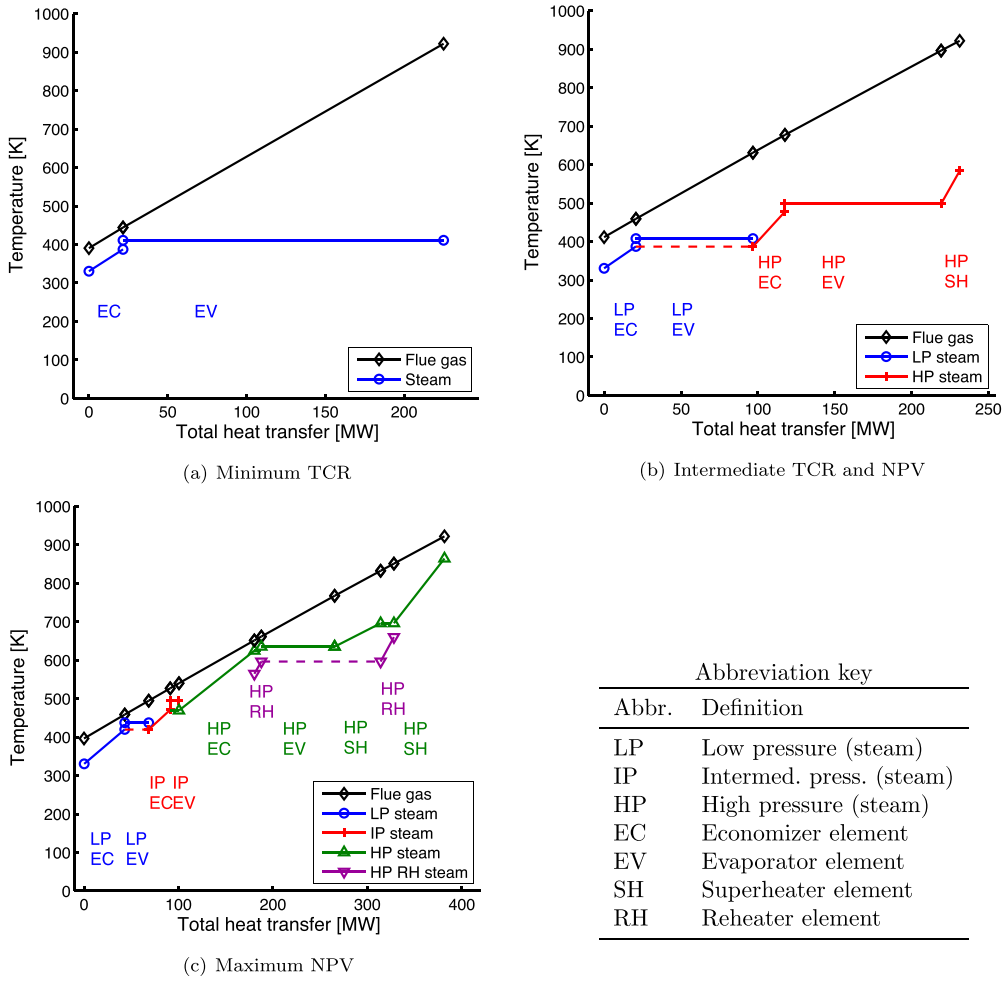

(a) Minimum TCR

(b) Intermediate TCR and NPV

(c) Maximum NPV

Abbreviation key

Abbr.	Definition
LP	Low pressure (steam)
IP	Intermed. press. (steam)
HP	High pressure (steam)
EC	Economizer element
EV	Evaporator element
SH	Superheater element
RH	Reheater element

Fig. 6. Temperature profiles of optimized HRSG designs in the base scenario (WTX-Base). Dashed lines indicate water bypass streams.

her specific preferences. A point on (rather than below) the frontier would always be chosen. Otherwise the solution selected would be suboptimal, since improvement in one of the objectives could be attained without any deterioration in the other objective by moving to the frontier.

The Pareto frontier obtained for the base scenario consists of 391 distinct solutions. The range of NPVs is \$93–198 million, and the range of TCRs is \$346–517 million. Subtracting from the NPV for the CP-only case, we find that in this scenario the net present cost of meeting the emission performance standard ranges from \$278 to 383 million. It is evident from Fig. 5 that the TCR and NPV objectives are in conflict, and that increased capital investment is required for increased NPV. The different objectives lead to noticeably different HRSG designs. The design associated with the minimum TCR solution (solid circle; NPV of \$93 million, TCR of \$346 million) corresponds to a one-pressure HRSG, while that for the maximum NPV solution entails a three-pressure HRSG (solid triangle; NPV of \$198 million, TCR of \$517 million).

A key advantage of resolving the full Pareto frontier is that intermediate, or 'compromise,' solutions can be identified. The best such solutions provide a significant improvement in one objective with only a minimal degradation in the other objective (as such, these solutions are often associated with sharp 'bends' in the frontier). One such intermediate solution (solid square) is identified in Fig. 5. This solution corresponds to a two-pressure HRSG and has an NPV of \$119 million and a TCR of \$351 million. This indicates that, relative to the minimum TCR solution, by investing an additional \$5 million in capital, we can achieve an increase of \$26 million in NPV.

With reference to Fig. 5, a general increase in the complexity of the HRSG, from one-pressure to two-pressure to three-pressure designs, is observed as we move along the Pareto frontier. The HRSG temperature profiles (in mode A) for the three highlighted designs are shown in Fig. 6. The one-pressure HRSG design in Fig. 6(a), which is the solution for minimum TCR, contains only two elements, while the three-pressure design (which maximizes NPV) in Fig. 6(c) is composed of 10 elements. The two-pressure intermediate design contains five elements. The area between the flue gas temperature profile and the (stair-step) steam-water profile is related to exergy destruction in the heat transfer operation. It is apparent that more complex (and more expensive) configurations lead to higher efficiencies, and thus more electricity generation.

In WTX-Base, the lowest partial load of the capture system in any Pareto-optimal design is 94.8%. A majority of Pareto-optimal designs do not use partial load at all, and of the optimal designs that do use partial load, the mean CO_2 capture partial load is 98.9%. System behavior at such high partial loads likely does not differ substantially from behavior at full load, so the assumption of negligible partial load efficiency loss for the CO_2 capture system (discussed in Section 3.2) is justified.

Fig. 7 displays the relationships between NPV and four major system parameters: total HRSG gas-side surface area, total GT generation capacity, CO_2 capture capacity, and CO_2 capture utilization factor. The first three parameters together indicate the size of the

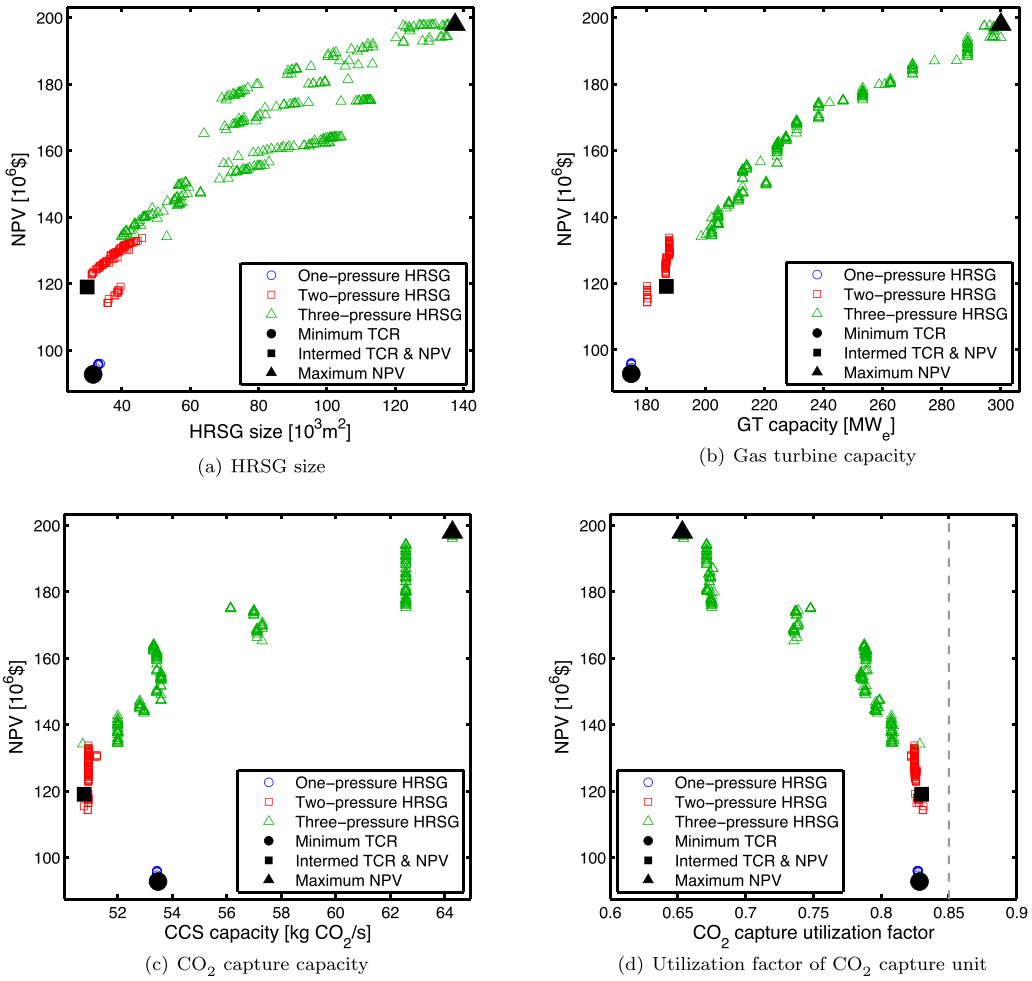

(a) HRSG size

(b) Gas turbine capacity

(c) CO_2 capture capacity

(d) Utilization factor of CO_2 capture unit

Fig. 7. Relationship between NPV and system parameters for Pareto-optimal designs in base scenario (WTX-Base).

auxiliary system that is constructed, while the CO_2 capture utilization factor is a metric for the planned operating profile of the facility. NPV increases with increasing size of the auxiliary retrofit system. The one-pressure HRSG systems indicated by the blue circles in Fig. 7(a) have greater CO_2 capture capacity than might be expected because the CCGT systems in these facilities are inefficient, so more CO_2 must be captured from the CP for the overall facility to meet the emission standard.

The relationships shown in Fig. 7 are not Pareto frontiers, since the quantities plotted along the *x*-axes are not objective functions. The relationship between NPV and HRSG size for Pareto-optimal systems, shown in Fig. 7(a), indicates that a given NPV can be achieved with several different HRSG sizes. One cause for this is that differences in non-HRSG variables across designs with similar HRSG sizes can have a large impact on NPV. In addition, the direct contribution of HRSG size to NPV (via capital cost) is relatively small. Furthermore, HRSG size is an aggregate measure of several HRSG design variables, so significantly different HRSG designs can be of the same size.

Facility operations also show clear trends. The CO_2 capture utilization factor is inversely related to NPV, as seen in Fig. 7(d). This indicates that higher NPV designs correspond to low (or zero) CO_2 capture rates during many hours of the year (recall that the maximum CO_2 capture utilization factor is 0.85 because the CP capacity factor is 0.85). The strike price operating profiles of the minimum TCR and maximum NPV systems are shown in Fig. 8 (the strike prices for the intermediate case are very close to those of the minimum TCR case). The system operates in mode D for more time in the NPV-maximizing case (Fig. 8(b)) than in the TCR-minimizing (and intermediate) cases (Fig. 8(a)). In fact, facilities toward the minimum-TCR end of the Pareto frontier are not designed to have flexibility with respect to the CO_2 constraint, so they must operate mostly in modes B and C to satisfy the constraint. Variation in CO_2 capture utilization is primarily associated with mode D duration, which is consistent with the fact that the CO_2 capture utilization factor is lowest for the NPV-maximizing system.

Several trends in Pareto-optimal systems can be seen in Figs. 7 and 8. Minimizing TCR leads to systems with lower CO_2 capture capacity, smaller CCGT systems, and greater utilization of CO_2 capture. Maximizing NPV favors facilities with higher CO_2 capture capacity, larger CCGT systems, and greater duration in mode D, in which both CO_2 capture and the CCGT system are inactive. The major reason for this behavior is that the NPV objective pushes the system to improve operational profitability by avoiding power generation during times with low power prices (as seen in the use of mode D in Fig. 8(b)), while the TCR objective is not affected by selling power at low prices. CCGT systems with greater generation capacity (larger GT and HRSG) appear in NPV-maximizing systems because the CCGT is profitable under the economic conditions used here. TCR minimization, by contrast, leads to the selection of a CCGT system with less generation capacity in part because profit earned from power generation does not contribute toward TCR.

The other three West Texas scenarios were optimized in the same manner as WTX-Base. A summary of results is presented in Table 3. The WTX-HighCapCost and WTX-HighEnergyCost scenarios exhibit many characteristics in common with each other and

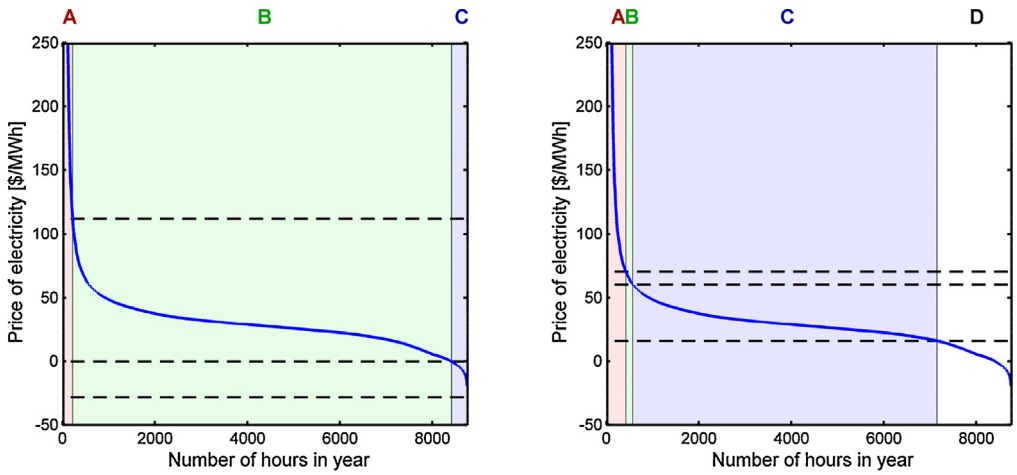

(a) Minimum TCR example strike prices (mode D usage is too small to see)

(b) Maximum NPV example strike prices

Fig. 8. Example operations of Pareto-optimal systems in the base scenario (WTX-Base).

with WTX-Base. Namely, these scenarios display Pareto frontiers with positive NPV (though the actual values differ greatly), indicating that a CCS retrofit would be preferred over decommissioning in the face of the CO_2 emission regulation (though we note that including transport and storage in saline aquifers, at a net present cost of approximately $47–249 million, may impact the economic viability of retrofits for WTX-Base and WTX-HighCapCost). Finally, it is of interest that the Pareto-optimal system parameters, shown in Table 3(b), in WTX-HighCapCost and WTX-HighEnergyCost exhibit similar ranges as in WTX-Base.

In contrast, the WTX-LowEnergyCost scenario exhibits quite different characteristics than the other West Texas scenarios, as seen in Table 3. The NPV in the WTX-LowEnergyCost scenario is negative for all points found (ranging from −$352 million to −$338 million), indicating that a CCS retrofit would not be preferred over decommissioning in this scenario. Additionally, the ranges of Pareto-optimal objective functions and system parameters are much narrower than in the other West Texas scenarios.

The fact that WTX-Base, WTX-HighEnergyCost and WTX-HighCapCost exhibit similar trends suggests that the optimized designs are in some sense robust with respect to realistic future scenarios. In other words, a facility designed for WTX-Base will not be highly suboptimal in either of the reasonably plausible scenarios of WTX-HighEnergyCost and WTX-HighCapCost. The WTX-LowEnergyCost scenario is unlikely to occur in a CO_2-constrained world, so the fact that results for this scenario indicate decommissioning is preferred should probably not be viewed as cause for concern.

7.3. United Kingdom and India

The UK results exhibit broadly similar trends to the WTX-Base results. The UK Pareto frontier shown in Fig. 9(a) has a similar overall shape as the WTX-Base Pareto frontier, and likewise demonstrates a clear conflict between the TCR and NPV objectives. Furthermore, the Pareto frontier structure is also similar, with one-pressure systems filling the low NPV region, three-pressure systems filling the middle and high NPV region, and two-pressure systems present in an intermediate region. Also of interest is that the UK Pareto frontier has both positive and negative NPVs. In this situation, the choice of objective could determine whether an auxiliary CO_2 capture retrofit is economically preferable to decommissioning, because a system designed to minimize TCR would not be economically viable, while a system designed to maximize NPV would be.

A key difference in the UK results as compared to the WTX-Base results is that flexibility plays a smaller role in the UK scenario than in WTX-Base. With reference to Table 3(b), the UK scenario

Table 3
Summary of scenario results.

(a) *Objective functions*

Scenario name	CP-only NPV [$10^6$$]	Pareto NPV range [$10^6$$]	Pareto TCR range [$10^6$$]
WTX-Base	476	93–198	346–517
WTX-HighCapCost	476	79–148	398–570
WTX-HighEnergyCost	836	423–589	348–519
WTX-LowEnergyCost	84	−352 to −338	342–347
UK	381	−73 to 105	331–481
India	1301	513–576	337–359

(b) *System parameters for Pareto-optimal systems*

Scenario name	GT capacity [MW]	HRSG gas-side surface area [10^3 m^2]	CCS capacity [kg CO_2/s]	CCS util. factor [%]
WTX-Base	175–300	29.3–137.5	50.7–66.3	65.3–83.1
WTX-HighCapCost	183–300	31.8–139.4	50.5–62.6	67.1–83.3
WTX-HighEnergyCost	182–300	25.4–159.5	50.6–62.6	67.1–83.6
WTX-LowEnergyCost	172–182	32.0–41.4	49.8–52.3	84.2–84.5
UK	173–300	23.8–193.2	48.5–50.7	82.8–84.9
India	169–186	30.4–58.7	49.5–51.9	83.2–84.2

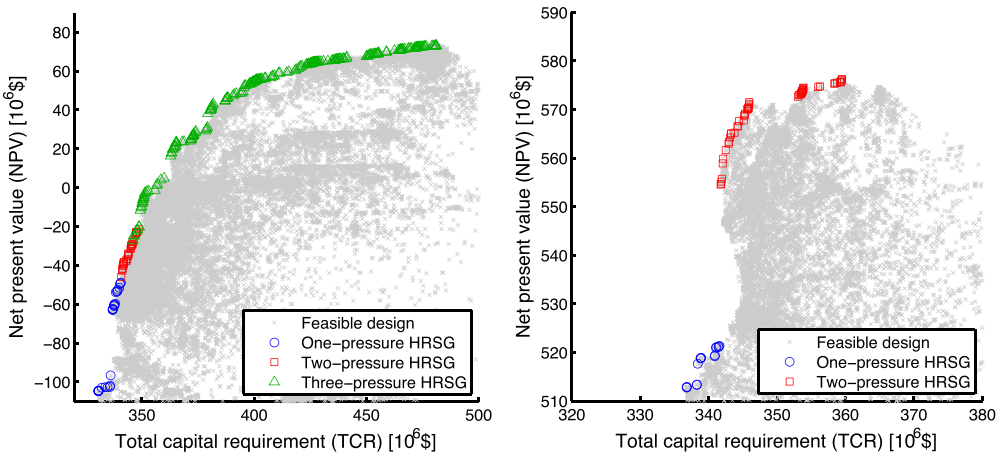

(a) United Kingdom (b) India

Fig. 9. Pareto frontiers for UK and India scenarios.

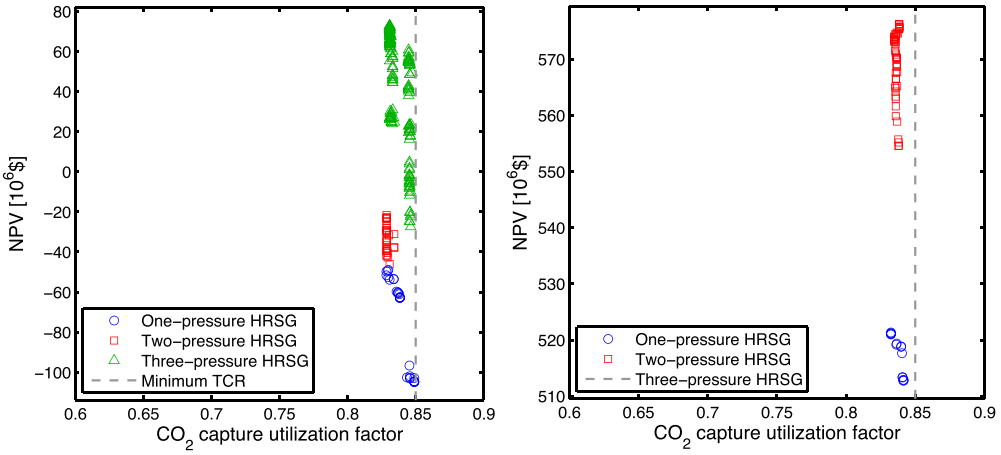

(a) United Kingdom (b) India

Fig. 10. CO_2 capture utilization factors of Pareto-optimal systems in UK and India scenarios.

includes HRSGs with greater total surface area than in WTX-Base. Additionally, the UK scenario exhibits a narrow range in CO_2 capture capacity, of 48.5–50.7 kg CO_2/s, in contrast to WTX-Base, which exhibits a range of 50.7–66.3 kg CO_2/s. These results indicate that systems in the UK scenario gain greater value from investment for high efficiency in the CCGT system (as seen in having larger HRSGs) than from investment for system flexibility (as seen in having lower CO_2 capture capacities). The decreased importance of flexibility is also seen in the absence of a correspondence between high NPV and low CO_2 capture utilization in Fig. 10(a) for the UK scenario. The strong association between lower CO_2 capture utilization and high NPV that is present in WTX-Base, as seen in Fig. 7(c), is not present in the UK scenario. The low importance of system flexibility is consistent with the fact that electricity price variability in the UK scenario (σ = \$13.53/MWh) is substantially less than in WTX-Base (σ = \$126.74/MWh); i.e., less electricity price variability leads to less value for flexibility.

The results for the India scenario differ greatly from WTX-Base. As seen in Fig. 9(b), the Pareto frontier consists only of one- and two-pressure systems, and spans a narrower range in both TCR and NPV than in WTX-Base. In fact, the range of TCR is similar to that in WTX-LowEnergyCost. Moreover, the ranges for the design parameters of Pareto-optimal systems in the India scenario are similar to those for WTX-LowEnergyCost, as seen in Table 3(b). The range in NPVs in the India scenario is narrower than in WTX-Base and wider than in WTX-LowEnergyCost. This indicates a lesser degree of conflict between the TCR and NPV objectives than in WTX-Base, but a greater degree of conflict than in WTX-LowEnergyCost. The NPVs found in the India scenario have highly positive values because of the high price of electricity and low price of coal in this case. However, the effective net present cost of the auxiliary gas-fired CO_2 capture retrofit in the India scenario is very large, \$725–788 million. This indicates that an auxiliary gas-fired CO_2 retrofit is a very costly way to mitigate CO_2 emissions in the India scenario.

As in the UK scenario, system flexibility in the India scenario is of lesser importance than in WTX-Base. This can be seen in Table 3(b), with the India results exhibiting similar CO_2 capture capacities and CO_2 capture facility utilization factors as in the UK results. This is further corroborated by the lack of a strong relationship between NPV and CO_2 capture utilization factor in the India scenario, as seen in Fig. 10(b). The low importance of system flexibility is consistent with low electricity price variability (σ = \$24.42/MWh) in the India scenario.

8. Conclusions and future work

In this work, we developed a modeling and optimization framework for designing hybrid coal–natural gas power plants with CO_2 capture, emphasizing heat integration and the design of the heat recovery steam generator (HRSG) in the gas-fired component of the

system. Our method treats facility design and operations as a bi-objective mixed integer nonlinear optimization problem. The two objectives are the minimization of total capital requirement (TCR) and the maximization of net present value (NPV). HRSG configuration is optimized in a novel way through the use of categorical (unordered discrete) variables. A recently developed PSO-MADS algorithm, which has not been applied previously for this type of problem, is used as the core optimization procedure. The overall approach is applicable to a broad range of energy problems, and may be particularly useful for systems with complex capital-operating tradeoffs and/or discrete variables.

Our model treats time-varying facility operation in a competitive electricity market using the electricity price–duration curve. Combined with component-by-component capital cost estimation, this enables us to optimize facility design and operations simultaneously. Using historical data, we constructed six scenarios (four based on West Texas, one based on the United Kingdom, and one based on India) and applied a 499 kg CO_2/MWh emission performance standard to reflect possible future regulation. A 440 MW coal plant undergoing a retrofit with an auxiliary natural gas-powered CO_2 capture process was considered. Computational optimization was used to produce Pareto frontiers for the six scenarios.

In the base scenario constructed from 2011 West Texas data, the two objectives were clearly in conflict, and systems on different portions of the Pareto frontier were noticeably different from one another. The TCR-minimizing system contained a one-pressure HRSG, a relatively small gas turbine, and a relatively small capacity for CO_2 capture. The NPV-maximizing system, by contrast, had a three-pressure HRSG, relatively large gas turbine capacity, and large capacity for CO_2 capture that enabled greater operational flexibility. These results highlight the strong impact of the decision maker's preference in objective function on the optimal design.

Two of the three West Texas sensitivity scenarios exhibited trends in objective functions and system parameters similar to those in the base scenario. These scenarios had the same or higher expected future energy prices (for both electricity and natural gas) relative to the base scenario. In contrast, the third West Texas sensitivity scenario indicated that CO_2 capture would be highly uneconomic under low energy prices.

The UK and India scenarios demonstrated the applicability of our method in worldwide contexts and further illustrated the importance of economic assumptions on optimal system design. The UK scenario results were broadly similar to those from the base West Texas scenario. Interestingly, the TCR-NPV Pareto frontier in the UK scenario displayed both negative and positive NPVs, which demonstrates that the choice of objective can affect the economic viability of a retrofit. The India scenario resulted in optimal system parameters that were similar to those for the West Texas low energy price scenario. The India scenario displayed positive NPVs but very large effective net present costs. This indicates that an auxiliary gas-fired CO_2 retrofit, although economically viable, may not be the best possible approach for CO_2 mitigation in the India scenario. Both the UK and India scenarios had lower electricity price variability than the West Texas scenarios, leading to a lesser degree of importance of flexibility in optimal system design.

The differences in results among the West Texas, UK and India scenarios illustrate the strong impact of the economic forecast on the optimal facility design. We note especially that forecasts of hourly-timescale electricity price variability, not just overall electricity price level, can have a significant effect on system design. The importance of economic forecasts, as observed here, is consistent with the findings of Khalilpour (2014), who indicated that optimal decisions for parasitic CO_2 capture retrofits are highly sensitive to forecasted CO_2 prices and other economic parameters.

Future work may include investigations of optimal systems in different market and regulatory environments, improved modeling and optimization of the CO_2 capture process, representation of system dynamics including transients, extensions to natural gas-only systems, and robust treatment of uncertainty in capital cost and energy prices.

Acknowledgements

We thank Obiajulu Isebor for help with the optimization algorithms, and Philip Brodrick for assistance with testing parts of the code and for useful discussions. We are also grateful to Christopher Edwards and Anthony Pavone for valuable conversations. The Stanford Center for Computational Earth and Environmental Science provided the computational resources used in this study. The first author thanks the Illich-Sadowsky Stanford Interdisciplinary Graduate Fellowship for financial support.

Appendix A. Supplementary Material (SM)

Supplementary Material (SM) associated with this article can be found, in the online version, at http://dx.doi.org/10.1016/j.ijggc.2014.09.019.

References

Abramson, M., Audet, C., Couture, G., Dennis Jr., J., Le Digabel, S., Tribes, C., 2014. The NOMAD Project (http://www.gerad.ca/nomad).

APX Group, 2014. UKPX RPD Historical Data (http://www.apxgroup.com/market-results/apx-power-uk/ukpx-rpd-historical-data/ accessed June 14).

Arce, A., Dowell, N.M., Shah, N., Vega, L., 2012. Flexible operation of solvent regeneration systems for CO_2 capture processes using advanced control techniques: towards operational cost minimisation. Int. J. Greenh. Gas Control 11, 236–250, http://dx.doi.org/10.1016/j.ijggc.2012.09.004.

Audet, C., Le Digabel, S., Tribes, C., 2009. NOMAD User Guide. Tech. Rep. G-2009-37, Les cahiers du GERAD (http://www.gerad.ca/NOMAD/Downloads/user_guide.pdf).

Audet, C., Svard, G., Zghal, W., 2008. Multiobjective optimization through a series of single-objective formulations. SIAM J. Optim. 19 (1), 188–210, http://dx.doi.org/10.1137/060677513.

Bassily, A.M., 2007. Modeling, numerical optimization, and irreversibility reduction of a triple-pressure reheat combined cycle. Energy 32 (5), 778–794, http://dx.doi.org/10.1016/j.energy.2006.04.017.

Berkenpas, M.B., Kietzke, K., Mantripragada, H., McCoy, S., Rubin, E.S., Versteeg, P.L., et al., 2009. IECM Technical Documentation Updates Final Report. Tech. Rep. DE-AC26-04NT41917. National Energy Technology Laboratory, Carnegie Mellon University, Pittsburgh, PA, USA (http://www.cmu.edu/epp/iecm/).

Brasington, R., Herzog, H., 2012. Dynamic response of monoethanolamine (MEA) CO_2 capture units. In: Carbon Management Technology Conference, Orlando, FL, USA, February 7–9, http://dx.doi.org/10.7122/151075-MS.

Budzianowski, W.M., 2012. Negative carbon intensity of renewable energy technologies involving biomass or carbon dioxide as inputs. Renew. Sustain. Energy Rev. 16 (9), 6507–6521, http://dx.doi.org/10.1016/j.rser.2012.08.016.

Casarosa, C., Donatini, F., Franco, A., 2004. Thermoeconomic optimization of heat recovery steam generators operating parameters for combined plants. Energy 29 (3), 389–414, http://dx.doi.org/10.1016/S0360-5442(02)00078-6.

Chen, Q., Kang, C., Xia, Q., 2010. Modeling flexible operation mechanism of CO_2 capture power plant and its effects on power-system operation. IEEE Trans. Energy Convers. 25 (3), 853–861, http://dx.doi.org/10.1109/TEC.2010.2051948.

Chalmers, H., Gibbins, J., 2007. Initial evaluation of the impact of post-combustion capture of carbon dioxide on supercritical pulverised coal power plant part load performance. Fuel 86 (14), 2109–2123, http://dx.doi.org/10.1016/j.fuel.2007.01.028.

Chalmers, H., Lucquiaud, M., Gibbins, J., Leach, M., 2009. Flexible operation of coal fired power plants with postcombustion capture of carbon dioxide. J. Environ. Eng. 135 (6), 449–458, http://dx.doi.org/10.1061/(ASCE)EE.1943-7870.0000007.

Cohen, S.M., Rochelle, G.T., Webber, M.E., 2010. Turning CO_2 capture on and off in response to electric grid demand: a baseline analysis of emissions and economics. J. Energy Resour. Technol. 132 (2), 021003, http://dx.doi.org/10.1115/1.4001573.

Cohen, S.M., Rochelle, G.T., Webber, M.E., 2012. Optimizing post-combustion CO_2 capture in response to volatile electricity prices. Int. J. Greenh. Gas Control 8, 180–195, http://dx.doi.org/10.1016/j.ijggc.2012.02.011.

Couper, J.R., Hertz, D.W., Smith, F.L., 2008. Process economics. In: Green, D.W., Perry, R.H. (Eds.), Perry's Chemical Engineers' Handbook, 8th ed. McGraw-Hill, New York, pp. 9-1–9-56.

Electric Reliability Council of Texas, 2013. Historical DAM Load Zone and Hub Prices (http://www.ercot.com/mktinfo/prices/ accessed July 13).

Energy Information Administration United States Department of Energy, 2012. Coal Transportation Rates to the Electric Power Sector (http://www.eia.gov/coal/transportationrates/ accessed June 14).

Energy Information Administration United States Department of Energy, 2013. Short-Term Energy Outlook Custom Table Builder Query (http://www.eia.doe.gov/emeu/steo/pub/cf_query/index.cfm accessed September 13).
Energy Information Administration United States Department of Energy, 2014. Coal News and Markets Archive (http://www.eia.gov/coal/news_markets/archive/ accessed June 14).
Environmental Protection Agency United States, 2013. Standards of Performance for Greenhouse Gas Emissions from New Stationary Sources: Electric Utility Generating Units (http://www2.epa.gov/sites/production/files/2013-09/documents/20130920proposal.pdf).
Farhat, K., Benson, S.M., 2013. A technical assessment of CO_2 interim storage in deep saline aquifers. Int. J. Greenh. Gas Control 15, 200–212, http://dx.doi.org/10.1016/j.ijggc.2013.02.018.
Federal Energy Regulatory Commission United States, 2013. FERC: Other Markets – LNG – Archives (http://www.ferc.gov/market-oversight/othr-mkts/lng/archives.asp accessed June 14).
Franco, A., Giannini, N., 2005. Optimum thermal design of modular compact heat exchangers structure for heat recovery steam generators. Appl. Therm. Eng. 25 (8–9), 1293–1313, http://dx.doi.org/10.1016/j.applthermaleng.2004.08.018.
Franco, A., Giannini, N., 2006. A general method for the optimum design of heat recovery steam generators. Energy 31 (15), 3342–3361, http://dx.doi.org/10.1016/j.energy.2006.03.005.
Franco, A., Russo, A., 2002. Combined cycle plant efficiency increase based on the optimization of the heat recovery steam generator operating parameters. Int. J. Therm. Sci. 41 (9), 843–859, http://dx.doi.org/10.1016/S1290-0729(02)01378-9.
Ganapathy, V., 1991. Waste Heat Boiler Deskbook. The Fairmont Press, Inc., Lilburn, GA, USA.
Gas Turbine World, 2010. GTW Handbook. Pequot Publishing, Southport, CT, USA.
Godoy, E., Benz, S.J., Scenna, N.J., 2011. A strategy for the economic optimization of combined cycle gas turbine power plants by taking advantage of useful thermodynamic relationships. Appl. Therm. Eng. 31 (5), 852–871, http://dx.doi.org/10.1016/j.applthermaleng.2010.11.004.
Grant, T., Morgan, D., Gerdes, K., 2013. Carbon Dioxide Transport and Storage Costs in NETL Studies. Tech. Rep. DOE/NETL-2013/1614. National Energy Technology Laboratory.
Harkin, T., Hoadley, A., Hooper, B., 2012a. Using multi-objective optimisation in the design of CO_2 capture systems for retrofit to coal power stations. Energy 41, 228–235, http://dx.doi.org/10.1016/j.energy.2011.06.031.
Harkin, T., Hoadley, A., Hooper, B., 2012b. Optimisation of power stations with carbon capture plants – the trade-off between costs and net power. J. Clean. Prod. 34, 98–109, http://dx.doi.org/10.1016/j.jclepro.2011.12.032.
Indian Energy Exchange Ltd., 2014. Area Prices (http://www.iexindia.com/marketdata/areaprice.aspx accessed June 14).
Internal Revenue Service United States Department of the Treasury, 2013. Publication 946: How to Depreciate Property (http://www.irs.gov/pub/irs-pdf/p946.pdf).
International Energy Agency Gas Coal and Power Division, 2012. Medium-Term Coal Market Report 2012. Tech. Rep.
Isebor, O.J., 2013. Derivative-Free Optimization for Generalized Oil Field Development, Ph.D. thesis. Stanford University.
Isebor, O.J., Durlofsky, L.J., Echeverria Ciaurri, D., 2013. A derivative-free methodology with local and global search for the constrained joint optimization of well locations and controls. Comput. Geosci. 18 (3–4), 463–482, http://dx.doi.org/10.1007/s10596-013-9383-x.
Isebor, O.J., Durlofsky, L.J., 2014. Biobjective optimization for general oil field development. J. Pet. Sci. Eng. 119, 123–138.
Islegen, O., Reichelstein, S., 2011. Carbon capture by fossil fuel power plants: an economic analysis. Manage. Sci. 57 (1), 21–39, http://dx.doi.org/10.1287/mnsc.1100.1268.
Jassim, M.S., Rochelle, G.T., 2006. Innovative absorber/stripper configurations for CO_2 capture by aqueous monoethanolamine. Ind. Eng. Chem. Res. 45 (8), 2465–2472, http://dx.doi.org/10.1021/ie050547s.
Kang, C.A., Brandt, A.R., Durlofsky, L.J., 2011. Optimal operation of an integrated energy system including fossil fuel power generation, CO_2 capture and wind. Energy 36 (12), 6806–6820, http://dx.doi.org/10.1016/j.energy.2011.10.015.
Kang, C.A., Brandt, A.R., Durlofsky, L.J., 2012. Impact of CO_2 emissions policy and system configuration on optimal operation of an integrated fossil-renewable energy park. In: Carbon Management Technology Conference, CMTC, Orlando, FL, USA, 7–9 February 2012, http://dx.doi.org/10.7122/151446-MS.
Kang, C.A., Brandt, A.R., Durlofsky, L.J., 2013. Optimal heat integration in a coal–natural gas energy park with CO_2 capture. Energy Procedia 37, 2715–2726, http://dx.doi.org/10.1016/j.egypro.2013.06.156 (11th International Conference on Greenhouse Gas Technologies (GHGT-11), November 18–22, 2012, Kyoto, Japan).
Kaviri, A.G., Jaafar, M.N.M., Lazim, T.M., Barzegaravval, H., 2013. Exergoenvironmental optimization of heat recovery steam generators in combined cycle power plant through energy and exergy analysis. Energy Convers. Manage. 67, 27–33, http://dx.doi.org/10.1016/j.enconman.2012.10.017.
Kays, W.M., London, A.L., 1984. Compact Heat Exchangers, 3rd ed. McGraw-Hill, New York.
Kehlhofer, R., Bachmann, R., Nielsen, H., Warner, J., 1999. Combined-Cycle Gas and Steam Turbine Power Plants, 2nd ed. PennWell, Tulsa, OK, USA.
Khalilpour, R., 2014. Multi-level investment planning and scheduling under electricity and carbon market dynamics: retrofit of a power plant with PCC (post-combustion carbon capture) processes. Energy 64, 172–186, http://dx.doi.org/10.1016/j.energy.2013.10.086.
Kim, T.S., 2004. Comparative analysis on the part load performance of combined cycle plants considering design performance and power control strategy. Energy 29 (1), 71–85, http://dx.doi.org/10.1016/S0360-5442(03)00157-9.
Le Digabel, S., 2011. Algorithm 909: NOMAD: Nonlinear optimization with the MADS algorithm. ACM Trans. Math. Softw. 37 (4), 1–15, http://dx.doi.org/10.1145/1916461.1916468.
Manassaldi, J.I., Mussati, S.F., Scenna, N.J., 2011. Optimal synthesis and design of heat recovery steam generation (HRSG) via mathematical programming. Energy 36 (1), 475–485, http://dx.doi.org/10.1016/j.energy.2010.10.017.
Mac Dowell, N., Shah, N., 2013. Identification of the cost-optimal degree of CO_2 capture: an optimisation study using dynamic process models. Int. J. Greenh. Gas Control 13, 44–58, http://dx.doi.org/10.1016/j.ijggc.2012.11.029.
Mansouri, M.T., Ahmadi, P., Kaviri, A.G., Jaafar, M.N.M., 2012. Exergetic and economic evaluation of the effect of HRSG configurations on the performance of combined cycle power plants. Energy Convers. Manage. 58, 47–58, http://dx.doi.org/10.1016/j.enconman.2011.12.020.
Martelli, E., Amaldi, E., Consonni, S., 2011. Numerical optimization of heat recovery steam cycles: mathematical model, two-stage algorithm and applications. Comput. Chem. Eng. 35 (12), 2799–2823, http://dx.doi.org/10.1016/j.compchemeng.2011.04.015.
Martelli, E., Nord, L.O., Bolland, O., 2012. Design criteria and optimization of heat recovery steam cycles for integrated reforming combined cycles with CO_2 capture. Appl. Energy 92, 255–268, http://dx.doi.org/10.1016/j.apenergy.2011.10.043.
Metz, B., Davidson, O., de Coninck, H., Loos, M., Meyer, L. (Eds.), 2005. IPCC Special Report on Carbon Dioxide Capture and Storage. Cambridge University Press, Cambridge, UK.
Mohagheghi, M., Shayegan, J., 2009. Thermodynamic optimization of design variables and heat exchangers layout in HRSGs for CCGT, using genetic algorithm. Appl. Therm. Eng. 29 (2–3), 290–299, http://dx.doi.org/10.1016/j.applthermaleng.2008.02.035.
Nellis, G., Klein, S., 2009. Heat Transfer. Cambridge University Press, New York.
Nord, L.O., Bolland, O., 2011. HRSG design for integrated reforming combined cycle with CO_2 capture. J. Eng. Gas Turbines Power 133 (1), http://dx.doi.org/10.1115/1.4001822, 011702-1–011702-7.
Norouzi, E., Mehrgoo, M., Amidpour, M., 2012. Geometric and thermodynamic optimization of a heat recovery steam generator: a constructal design. J. Heat Transf. 134, http://dx.doi.org/10.1115/1.4007070, 111801-1–111801-12.
Pelster, S., 1998. Environomic Modeling and Optimization of Advanced Combined Cycle Cogeneration Power Plants Including CO_2 Separation Options. Ph.D. thesis. Ecole Polytechnique Federale de Lausanne (Thesis No 1791).
Pelster, S., Favrat, D., von Spakovsky, M.R., 2001. The thermoeconomic and environomic modeling and optimization of the synthesis design and operation of combined cycles with advanced options. J. Eng. Gas Turbines Power 123 (4), 717–726, http://dx.doi.org/10.1115/1.1366323.
Ragland, A., Stenzel, W., 2000. Combined cycle heat recovery optimization. In: Proceedings of the 2000 International Joint Power Generation Conference, Miami Beach, FL, USA, July 23–26, 2000. ASME (IJPGC2000-15031).
Rubin, E., Berkenpas, M., Zaremsky, C., 2007. User Manual: Integrated Environmental Control Model (http://www.cmu.edu/epp/iecm/).
Shah, R.K., Sekulic, D.P., 2003. Fundamentals of Heat Exchanger Design. John Wiley & Sons, Hoboken, NJ, USA.
Ulrich, G.D., Vasudevan, P.T., 2004. Chemical Engineering Process Design and Economics: A Practical Guide, 2nd ed. Process Publishing, Durham, NH, USA.
Ulrich, G.D., Vasudevan, P.T., 2009. Capital costs quickly calculated: estimating capital costs early can prevent unnecessary expenditures on dead-end projects. Chem. Eng. April, 46–52.
Versteeg, P., Oates, D.L., Hittinger, E., Rubin, E.S., 2013. Cycling coal and natural gas-fired power plants with CCS. Energy Procedia 37, 2676–2683, http://dx.doi.org/10.1016/j.egypro.2013.06.152 (11th International Conference on Greenhouse Gas Technologies (GHGT-11), Kyoto, Japan, November 18–22, 2012).
Woudstra, N., Woudstra, T., Pirone, A., van der Stelt, T., 2010. Thermodynamic evaluation of combined cycle plants. Energy Convers. Manage. 51 (5), 1099–1110, http://dx.doi.org/10.1016/j.enconman.2009.12.016.
Yang, A., Cui, Y., 2012. Global coal risk assessment: data analysis and market research. WRI Working Paper. World Resources Institute, Washington DC, USA (http://www.wri.org/sites/default/files/pdf/global_coal_risk_assessment.pdf).
Zhao, Y., Chen, H., Waters, M., Mavris, D.N., 2003. Modeling and cost optimization of combined cycle heat recovery generator systems. In: Proceedings of ASME Turbo Expo 2003 Power of Land, Sea, and Air, June 16–19, Atlanta, GA, USA (ASME-GT-2003-38568, http://hdl.handle.net/1853/6362).
Ziaii, S., Cohen, S., Rochelle, G.T., Edgar, T.F., Webber, M.E., 2009a. Dynamic operation of amine scrubbing in response to electricity demand and pricing. Energy Procedia 1, 4047–4053, http://dx.doi.org/10.1016/j.egypro.2009.02.211 (9th International Conference on Greenhouse Gas Control Technologies (GHGT-9), Washington DC, USA, November 16–20, 2008).
Ziaii, S., Rochelle, G.T., Edgar, T.F., 2009b. Dynamic modeling to minimize energy use for CO_2 capture in power plants by aqueous monoethanolamine. Ind. Eng. Chem. Res. 48 (13), 6105–6111, http://dx.doi.org/10.1021/ie801385q.